Bundling and Diameter Selectivity in HiPco SWNTs Poly(*p*-phenylene vinylene-*co*-2,5-dioctyloxy-*m*-phenylene vinylene) Composites

S. M. Keogh,*,† T. G. Hedderman,† P. Lynch,‡ G. F. Farrell,§ and H. J. Byrne†

FOCAS Institute/School of Physics, Dublin Institute of Technology, Kevin Street, Dublin 8, Ireland, FOCAS Institute/School of Chemistry, Dublin Institute of Technology, Kevin Street, Dublin 8, Ireland, and Letterkenny Institute of Technology, Letterkenny, County Donegal, Ireland

Received: November 2, 2005; In Final Form: June 27, 2006

Temperature-dependent (TD) Raman measurements at laser excitation 514.5 nm were performed at different concentrations. The spectral profile of the radial breathing modes were investigated up to a polymer concentration of 1 g/L and were found to be dominated by ∼1.2−1.4 nm diameter tubes at room temperature. Upon heating above the glass transition of the polymer (60 °C) the smaller tubes around ∼0.9 nm increased significantly in relative intensity. This suggests that below the glass transition of the polymer (60 °C) RBMs within the composite are damped and spectral changes cannot be interpreted as diameter selective solubilization. The observed RBM damping at room temperature only occurred up to a concentration of $\sim 1.2 \times 10^{-4}$ g/L and below this no damping was observed. Photoluminescence intensity (PL) measurements were taken for a range of PmPV concentrations, in which HiPco single walled carbon nanotubes (SWNTs) at 100%, 10%, 1%, 0.1%, 0.01%, and 0% mass fractions were added. Fitting of the concentration dependence to a dynamic absorption/desorption model indicates that the polymer interacts with nanotube bundles until a critical concentration of $\sim 1.2 \times 10^{-4}$ g/L is reached, below which the nanotubes are isolated. The polymer and or solvent has a significant effect on the debundling and aggregation within these systems. Aggregation and/or interaction with the polymer at higher concentrations can effect the RBM profile in the composite at ambient temperatures, providing an incomplete representation of the selection of diameters present within composites at a particular wavelength.

1. Introduction

Currently, there is great interest in exploiting the properties of SWNT by incorporating carbon nanotubes into a wide variety of composites, including starch,[1] ceramics,[2] oligimers,[3] and polymers.[4−9] In each system, formation of a well-dispersed, stable composite with significant mechanical and physical property enhancement is desired. It has previously been shown at ambient temperatures that SWNTs upon interaction with the organic semiconjugated polymer *p*-phenylene vinylene-*co*-2,5-dioctyloxy-*m*-phenylene vinylene (PmPV) allow solubility and diameter selective purification of nanotubes.[4] It is proposed that the PmPV backbone reorganizes into a relatively flat helical structure due to the *m*-phenylene linkage and repulsive interaction between the octyloxy side groups.[10] The exposure of the backbone plays an important role in facilitating dipolar binding between the polymer and the nanotube, allowing the polymer to π stack onto the nanotube backbone.[10] The cis to trans ratio has been shown to be a critical parameter affecting the solid-state morphology of the polymer, where increasing the trans content leads to higher backbone ordering of the polymer.[11] Recent temperature studies have shown that carbon nanotubes nucleate crystallinity in polymers such as polypropylene,[12,13] poly(vinyl alcohol),[14] and PmPV.[15] In particular we have investigated the temperature dependence of the G-line of both PmPV and the HiPco composite.[16] We have shown that temperature cycling facilitates a change in isomerization above the glass transition temperature of the polymer, resulting in an increased polymer tube backbone binding.[16]

Raman spectroscopy has been demonstrated to be a key technique for the characterization of SWNTs. This is because of the strong resonant enhancement of the RBMs with respect to tube diameters. Application of this technique has been repeatedly demonstrated.[17−21] The RBM Raman frequency position is known to be upshifted because of intertubule interaction in bundles and the degree of frequency upshift has been shown to depend on the bundle size.[22,23] Other studies have investigated the systematic changes to the RBM Raman intensity to variation in the degree of aggregation within SWNT samples.[24] Here Heller at al. reported that aggregation shifts the effective excitation profile and causes peaks to increase or decrease, depending on where the transition lies relative to the excitation wavelength.[24] Their findings are particularly relevant for evaluating size selectivity in samples. In this paper we investigate the dependence of the diameter selective solubilization on composite solution concentration. As has been demonstrated by Coleman et al. for a similar composite, the solution concentration is a critical parameter in the interaction of the polymer with the nanotubes.[25] It is shown that only below a critical concentration (C_o) is debundling and consequently diameter selective solubilization of the nanotubes affected. Although at all concentrations a degree of selectivity is suggested by the changes in the Raman Radial Breathing Mode (RBM) spectra compared with pristine nanotubes, temperature-dependent studies show that above the critical debundling

* Address correspondence to this author. E-mail: sinead.keogh@dit.ie.
† FOCAS Institute/School of Physics.
‡ FOCAS Institute/School of Chemistry.
§ Letterkenny Institute of Technology.

10.1021/jp056321k CCC: $33.50
Published on Web 09/06/2006

concentration the spectral changes are due to vibrational damping in bundles.

Although absorption spectroscopy has been shown to examine SWNT in water-based solutions,[26] in composites with conjugated polymers, the absorption of the polymer dominates the spectrum in the visible region. To investigate the bundle size in our composite, therefore, we utilize an approach by Coleman et al. that measures the fluorescence of the polymer in the composite.[25] The fluorescence of the nanotubes within the composite was not measured in the near-infrared region as this region was not accessible with the available instrumentation. Furthermore, it has been demonstrated that the polymer fluorescence is an extremely sensitive probe of the aggregation state of the nanotubes in composite solutions.[25] The maximum photoluminescence (PL) intensity yield of the polymer was shown to decrease upon introduction of nanotubes. This decrease has been reported previously and is attributed to a nonradiative decay of the photogenerated excitons into the many vibrations of the nanotubes backbone.[25] Therefore, for low polymer concentrations, increasing the nanotube mass fraction within the composite decreases the PL emission yield, as more polymer becomes quenched as a result of interaction with the nanotube backbone. Coleman et al. derived a model based on adsorption/desorption kinetics for the composite.[25] Here the ratio of the maximum PL intensity of the composite, which includes both bound and unbound polymer chains, and the maximum PL intensity of the polymer, which includes only unbound polymer chains, was plotted as a function of polymer concentratin.[25] In a 1:1 ratio (or 100% mass fraction by weight) composite, it was shown that as the composite concentration is lowered the bundles break up until isolated SWNTs are stable at low concentrations. Atomic force microscopy (AFM) confirmed individual nanotubes are stable in solutions below 3×10^{-5} kg/m^3.[25] As well as developing a new method for controlled debundling of SWNTs in solution, indirectly a binding energy of $\sim$1.1 eV was calculated from a derived binding scheme.[25] This model is limited to low polymer concentrations only and is not applicable at high polymer concentrations as here the chains can interact with themselves, or other chains, to form aggregates, which also cause a decrease in fluorescent yield.

In this study composites of the organic semiconjugated polymer PmPV and HiPco SWNT are explored by using temperature-dependent Raman spectroscopy in conjunction with fluorescence spectroscopy. As reported previously with Raman spectroscopy the G-line of the composite becomes abruptly dominated by nanotubes above the T_g (60 °C) of the polymer.[16] Here we show the change in local environment and or aggregation state of the composite by changes to the spectral profile of the radial breathing modes for the composites under examination. Fluorescence measurements of the polymer are used to probe the bundle size of SWNTs in various concentrations of PmPV. We show that when the tubes are isolated at low concentrations, changes in the aggregation state do not affect the RBM profile indicating isolated size selective interaction at low concentration. A range of mass fractions, including 0.01%, 0.1%, 1%, 10%, and 100%, are characterized to determine what influence the SWNT mass fraction has on the bundle size as a function of polymer concentration. Comparing our system to that of Coleman et al. indicates that the choices of composite, i.e., polymer, and solvent have an impact on bundling within these composites.

2. Materials Preparation

The HiPco SWNTs used in this study were purchased from CNI Houston, and were used without further treatment. The nanotubes were solubulized in toluene, to form composites with poly(*p*-phenylene vinylene-*co*-2,5-dioctyloxy-*m*-phenylene vinylene), which was synthesized in house, via the Horner-Emmons polycondensation in dimethylformaide (DMF) as described in ref 27. Gel permeation chromatography with polystyrene standards shows a weight average molecular weight (M_w) of 17 200 and a number average molecular weight (M_n) of 6 500 giving a polydispersivity M_w/M_n of 2.65.[28]

Raman spectra were obtained with an Instruments SA LabRam 1B system. The confocal imaging system uses either a He−Ne laser at 632.8 nm or an argon ion laser at 514.5 nm. The laser power was set to $\sim$1.3 mW at the sample and was focused into a spot size of 1−2 μm in diameter, giving a power density of about 3×10^4 W/cm^{-2}. The system was fitted with a Linkam LNP cooling stage to perform temperature-dependent measurements. The LNP system was used in conjunction with a THMS 600 stage to cool and heat samples as desired. This instrument has a heating and cooling range of −196 to 300 °C, and when water-cooled is capable of reaching temperatures up to 600 °C. To aid thermalization Raman measurements were held for 10 min at each temperature, prior to data acquisition, which was set to 30 s in each case.

For fluorescence measurements a 2 g/L stock solution of PmPV in toluene was first prepared, and then split into two identical solutions. To one solution of polymer, HiPco SWNTs of 100% mass fraction (by weight) was added to form a polymer tube mass ratio of 1:1. Both solutions were continually diluted by a factor of 2, to produce a concentration range of 2 g/L to 5.95×10^{-8} g/L, ensuring that the partial polymer concentration in the composite solutions was the same as the polymer concentrations in the corresponding polymer solutions. Each solution was sonicated for 10 s with a high-power Branson ultrasonic tip, and allowed to settle for 24 h to allow insoluble material to precipitate to the bottom. Sediment was observed for high polymer concentrations so the supernatant was pipetted into additional sample bottles. This sample preparation procedure was also carried out for SWNT mass fractions of 10%, 1%, 0.1%, and 0.01%. Fluorescence measurements were carried out with a 10 mL quartz cell and recorded on an LS55B Perkin-Elmer luminescence spectrometer. Samples were excited at 330 nm and recorded in the wavelength range of 340 to 650 nm. First, the fluorescence spectra of PmPV in the concentration range of 2 g/L to 5.8×10^{-8} g/L was measured and the maximum emission yield in each was recorded. Second, the fluorescence spectra for each composite in the same concentration range was measured and the maximum emission yield in each case was also recorded. Third, the intensity of polymer N_F (unbound polymer) divided by the intensity of the composite $N_F + N_B$ (unbound polymer + bound polymer) was calculated and graphed as a function of polymer concentration. From this relationship the concentration at which the bundles break up can be ascertained.

3. Results and Discussion

The Raman spectra of SWNTs are dominated by two features. The first is the G-line, which is strongly related to the tangential mode in graphite and is centered round 1590 cm^{-1}.[29] The second is the radial breathing modes (RBM) positioned between $\sim$140 and 220 cm^{-1}, and only they will be considered in this study.[29] A number of authors have theoretically calculated the diameter dependence of the radial breathing mode frequency ω_{RBM} for isolated SWNTs and have used the functional form ω_{RBM} (cm^{-1}) $= A/d$ (nm) where d is the SWNT diameter and A is a constant. In the following discussion, the Kukovecz model is applied to

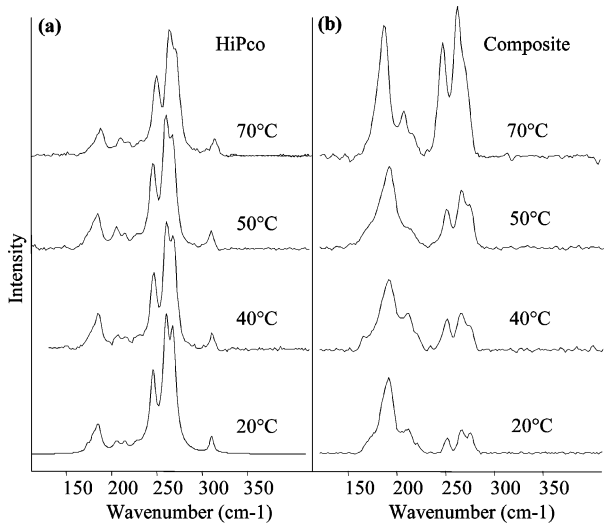

Figure 1. (a) Tempeature-dependent Raman at excitation wavelength 514.5 nm for (a) HiPco and (b) HiPco/PmPV composite (0.1 wt % mass fraction of SWNT in 1 g/L of PmPV).

determine the diameters present in the HiPco samples where ω_{RBM} (cm^{-1}) = 239/d (nm) + 8.5 cm^{-1}.[20] This value is complicated further in the composites due to the presence of the polymer. In the spectra of the composites, peaks which are obviously shifted from their positions within the raw material are assigned to the same diameters. Thus, this has been modified for the HiPco composites to be $\omega_{RBM} = (239/d\ (nm)) + \Gamma$, where Γ represents the diameter-independent approximation resulting from the environment of the tubes and is 8.5 cm^{-1} for HiPco soot. For polymer−tube systems Γ is 11.5 cm^{-1} for HiPco composites.[30] It is noted that the RBM position and shape is determined by the resonant enhancement of certain tubes at the wavelength of the source laser.[20]

Much research has been carried out on the temperature dependence of raw tubes and it has been shown that the position and profile of all Raman modes are highly temperature dependent.[31−37] The observed downshift in the RBMs has been attributed to thermal expansion in the radial direction, softening of the C−C intratubular interaction, and softening of the van der Waals intertubular interaction in SWNT bundles.[34] The latter two are reported to be the primary contributors to this downshift.[34] In this study we carry out thermal measurements using an external heating device, although groups have reported taking temperature measurements by varying the intensity of the laser.[32] Li et al. have compared both these procedures and have shown that downshifts in the nanotube mode frequencies induced by laser heating are basically identical with those induced by an external heating device.[32] To avoid induced laser heating of our samples the power density of the laser was kept low at ∼3 × 10^4 W/cm^2. Raravikar et al. have reported minimal heating effects at laser power density 3 × 10^5 W/cm^2.[34]

To ensure that our system was not overheating we calculated the temperature coefficient of Raman frequency shift, dω/dT, in the temperature range of −100 to +100 °C to be −0.0180 cm^{-1}/°C for the highest intensity GM mode at 1590 cm^{-1}, which is close to the previous presented value of −0.0189 cm^{-1}/°C.[34] Although the temperature dependence of SWNTs has been well established, here we propose to investigate the temperature dependence of the RBMs of our HiPco/PmPV composite employing excitation frequencies of 514.5 nm for the raw tubes and the composite. In Figure 1a the RBMs are presented for the raw HiPco sample at four temperatures between 20 and 60 °C. Although there is an observed downshift of about 0.5 cm^{-1}

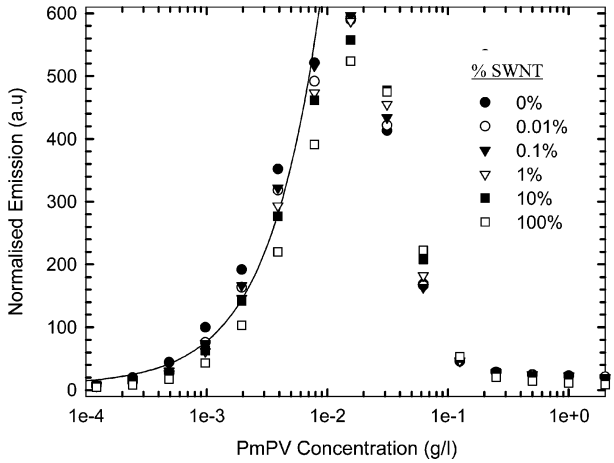

Figure 2. Maximum emission intensity of PmPV and SWNT/PmPV composite at 0%, 0.01%, 0.1%, 1%, 10%, and 100% mass fractions by weight.

there is no change in the relative intensity of the modes upon increase in temperature and upon cooling the shift is reversible. For temperatures of ∼700 K irreversible changes in the Raman spectrum have been reported due to thermal annealing of structural defects in the samples and a burning of the smaller diameter nanotubes.[37] In Figure 1b the spectrum at 20 °C is similar to that reported previously at ambient temperatures for this composite.[30] There are no significant spectral changes to the RBM spectrum up to 50 °C indicating no change in the aggregation state or local environment; however, at 70 °C changes are observed in the relative intensity of the RBM region indicating changes to the local environment. This can be explained as the T_g of the polymer occurs ∼60 °C and therefore impacts on the interaction between the polymer and the SWNT bundles.[16] This would suggest that the smaller tubes are damped either by tube−tube interaction or by polymer−tube interaction at room temperature at this concentration. It further highlights that an apparent diameter selective solubilization of the tubes is in fact a damping of the breathing modes of certain tube diameters.

To obtain samples of isolated or small bundles of tubes we exploit the approach taken by Coleman et al. as described above by utilizing the fact that PmPV is highly luminescent and therefore is a suitable material for fluorescence spectroscopy. The fluorescence spectrum for many PPV derivatives, including PmPV, has been well documented.[11,38] The concentration dependence of PmPV is discussed in refs 11 and 39. The position and emission yield of the main peaks at 330 and 420 nm are highly concentration dependent.[39] In Figure 2 the maximum PL intensity for PmPV and each composite was as a function of PmPV concentration plotted on a semilogarithmic plot for clarity. It is observed that the emission yield of PmPV increases up to a concentration of to 3.9 × 10^{-3} g/L, after which a further increase in concentration results in a decrease in intensity. It has been shown that this decrease in emission yield is accompanied by an apparent red shift and formation of a new emission feature at 530 nm resulting from aggregate formation.[11] The apparent red shift has been shown to be the result of the emergence of an aggregate absorption on the low-energy side of the polymer absorption. The long-wavelength emission has been shown to be an emission from this aggregate species.[11] It has been shown that this aggregation in polymers at high concentrations has a detrimental effect on the emission yield and incorporation of carbon nanotubes is one possible route for control of interchain interaction at high polymer concentrations.

In Figure 2 a decrease in fluorescent yield was recorded for all composite samples up to a concentration of 1.56×10^{-3} g/L, upon introduction of nanotubes. This has been reported previously for Arc-Discharge MWNT/PmPV composites.[15] It is thought that the nanotubes act as a template upon which the polymer self-assembles. Ryan et al. have proposed a linear relationship between volume fraction and PL intensity, for small loading fractions of MWNTs in PmPV.[15] It was suggested that at loading fractions above 0.03%, this relationship is no longer linear due to the coalescence of adjacent crystalline regions and nanotube aggregation. As the polymer mass fraction increases above 1.56×10^{-3} g/L an increase in fluorescence yield upon introduction of all mass fractions of nanotubes is observed. Dalton et al. have reported a similar behavior at high concentrations for Arc-Discharge MWNT/PmPV composites. Here it was shown for a 1×10^{-4} M (4.6×10^{-2} g/L) solution of PmPV in toluene that loading fractions up to 7% resulted in an increase in intensity. They suggested that at low mass fractions there is an initial increase in fluorescence as addition of MWNTs mimics the reduction in polymer concentration. It was also suggested that the nanotubes act as nanospacers, isolating the polymer strands from each other, thus preventing the formation of aggregates. Saturation was observed at 9%, where a decrease in intensity was again observed. [11] The concentration dependence of the emission maximum was fit and shows a linear relationship obeying the Beer Lambert law up to $\sim 1 \times 10^{-2}$ g/L, and then departs from ideal behavior because of the formation of aggregates.

Although in Figure 2 a systematic decrease in PL intensity was observed upon increasing the mass fraction up to a concentration of 1.56×10^{-3} g/L and a systematic increase in PL intensity was observed at 6.25×10^{-2} g/L upon introduction of nanotubes, this relationship does not always exist. For example, at 3.13×10^{-3} g/L the 10% mass fraction is at a greater PL intensity compared to the 100% mass fraction. This would suggest a saturation of the 100% mass fraction at this concentration. Therefore, the optimum PL intensity for a PmPV concentration of 6.25×10^{-3} g/L is obtained by incorporation of a mass fraction of 100% SWNTs. Above 2.5×10^{-1} g/L the PL intensity of the 100% and 10% composites is greatly reduced, due to the saturation of nanotubes at high SWNT/polymer concentration. Sediment was observed in the 100% mass fraction samples up to a polymer concentration of 1.25×10^{-3} g/L, which also implies nanotube saturation.

As discussed in the Introduction, Coleman et al. have employed fluorescence spectroscopy to study polymer−nanotube absorption/desorption kinetics. This technique utilized the luminescent properties of two semiconjugated polymers, poly[*p*-phenylene vinylene-*co*-(1,5-dioctyloxy-2,6-naphthylene vinylene)] (ppNV) and poly[*m*-phenylene vinylene-*co*-(1,5-dioctyloxy-2,6-naphthylene vinylene)] (pnNV), to measure the fraction of unbound polymer as a function of concentration for composite solutions in chloroform.[25] Coleman et al. presented a model for low polymer concentrations and when the system is in equilibrium they suggested that the adsorption rate equals the desorption rate. The adsorption rate is calculated theoretically; representing a nanotube bundle as a cylinder and it is assumed any molecule, which reaches the bundle, adsorbs by a van der Waals interaction. The desorption rate was shown to follow first order kinetics and was calculated as a function of the number of bound molecules per unit volume, volume of solution occupied by one bundle, binding energy, and most importantly to our study the bundle surface area.[25] As the fraction of free polymer changes over the concentration range

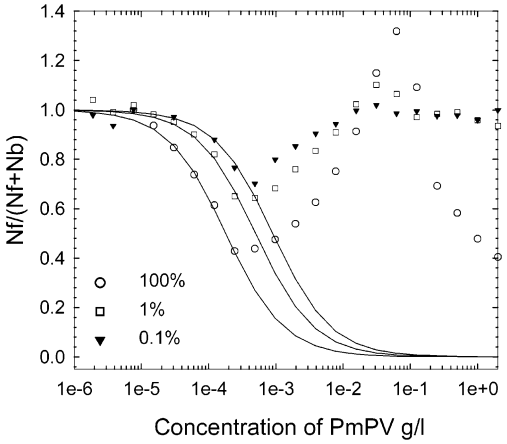

Figure 3. Graph of the fraction of free polymer for 100, 1, and 0.01 wt % composites as a function of concentration for PmPV, where N_f and N_b are the number of free and bound polymer molecules, respectively.

studied at equilibrium they arrived at a relationship where the change in fraction of free polymer could be described by a characteristic concentration C_o and the nanotube concentration C_{NT}, where N_f is the fraction of free polymer and N_b is the fraction of bound polymer.[25]

$$\frac{N_f}{N_f + N_b} = \frac{1}{1 + C_{NT}/C_o} \tag{1}$$

The fraction of free polymer was calculated from the ratio of the intensities of the composite PL to the polymer PL, and is presented in Figure 3. From this C_o, the characteristic concentration, could be obtained for each presented mass fraction. The characteristic concentration contains contributions from SWNT/polymer geometry, diffusion coefficient, binding energy, etc., and is described in ref 25. For a 100% mass fraction a C_o value of 2.2×10^{-5} kg/m^3 was obtained and essentially below this concentration individual nanotubes are present in solution. This was confirmed by AFM.[25]

In the higher concentration region ($\sim 10^{-1}$ g/L), the polymer is substantially aggregated, as demonstrated by the departure from linearity and decrease in PL intensity in Figure 2. In Figure 3, the 100% and 1% mass fractions are substantially greater than one in the region of 6.25×10^{-2} g/L. Any increase in PL emission yield because of the presence of nanotubes is due to a decrease in aggregation within the polymer, which results in an effective local dilution. Thus the apparently conflicting trends observed in Figure 2 can be understood in terms of three regions as characterized by the existence and interaction of free polymer and isolated nanotubes, free polymer and nanotube aggregates of varying size, and polymer aggregates with nanotube aggregates.

This was not observed for the concentration range studied by Coleman et al. This can be due to a number of parameters; for example, the polymer and solvents used were different. Chloroform is nonaromatic and such solvents have been shown previously to reduce aggregate formation of aromatic polymers until higher concentrations.[38] Toluene on the other hand promotes aggregation and consequently provides an environment in which the tubes can have an affect on the emission yield of the polymer. The 0.01% mass fraction is relatively flat in this region and this suggests that there is not a sufficient number of tubes within the composite to prevent aggregate formation at the concentrations studied. Considering the analysis of Coleman et al., in conjunction with the aggregation studies, this region,

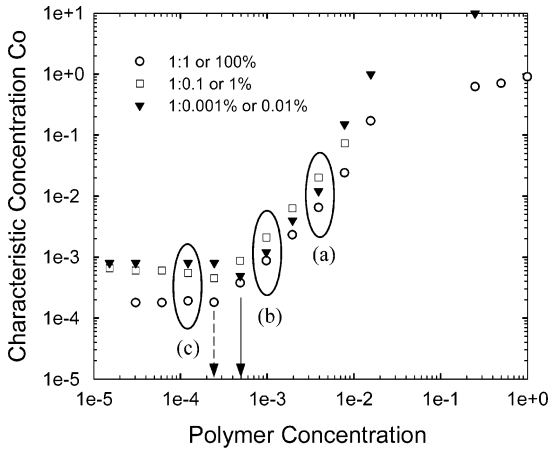

Figure 4. Graph of characteristic concentration for the 100%, 1%, and 0.01% mass fraction of SWNTs as a function of PmPV. The broken arrow shows the C_o value for the 100 wt % mass fraction of SWNTs and the solid arrow shows the C_o for the 0.01 wt % mass fraction SWNTs.

for all mass fractions, is characteristic of nanotube bundles partially de-aggregating the polymer material.

Below $\sim 5 \times 10^{-2}$ g/L, the concentration dependence of the PL in Figure 2 is linear, and the polymer exists in solution as isolated strands. However, the concentration dependence of the PL ratio does not fit well to eq 1. It has been shown that this is because the combination of interaction with polymer and solvent is not sufficient to break up the nanotube bundles. In this region the polymer PL is quenched by interaction with the bundles. At any fixed concentration, however, the degree of quenching is not linearly dependent on nanotube mass fraction indicating the complexity of the dynamic interactions as the concentration is reduced toward $\sim 4 \times 10^{-4}$ g/L. The isolated polymer strands progressively intercalate into the nanotube bundles, isolating the nanotubes from each other, until saturation is reached and all tubes are isolated. Below this point, a dynamic equilibrium between isolated nanotubes and polymer and bound nanotube/polymer composite exists. This equilibrium was modeled as in eq 1 for the 1:1 ratio and C_o was calculated to be $\sim 1.8 \times 10^{-4}$ g/L as shown Figure 4. This would suggest that PmPV in toluene is more effective at breaking up nanotube bundles compared to either of those polymers studied by Coleman et al.[25] As the binding energy is expected to be in the same region for our composite, this difference in C_o can possibly be accounted for because of the difference in hydrodynamic radius of PmPV. Studies of interaction with organic dye systems have also shown that this C_o is highly dependent on the type of tube used in the composite.[40] It is noted that the 1% and 0.01% appear to reach the point of inflection (complete debundling) at a higher polymer concentration. This is not surprising as the lower mass fractions are more dispersed and the bundles are smaller. Previous Raman spectroscopy results for 1%, 0.1%, and 0.01% mass fractions of SWNTs in PmPV (1 g/L) showed a significant change to the G-line spectral region.[30] A narrowing of the G-line was observed in each case and is associated with a decreased interaction between individual tubes. For the HiPco composite the greatest G-line shift was observed from the 0.1% to 1% mass fractions, indicating a breaking of large bundles within the composite at the 0.1% mass fraction.[30] This results in a differing fit of eq 1, and thus different values of C_o for the lower mass fractions. For the 1% and 0.01% mass fraction C_o was calculated to be $\sim 5 \times 10^{-4}$ and $\sim 8.5 \times 10^{-4}$ g/L, respectively. Although the variation in C_o is small, a notable difference is observed and is graphed in Figure 4. The model used was

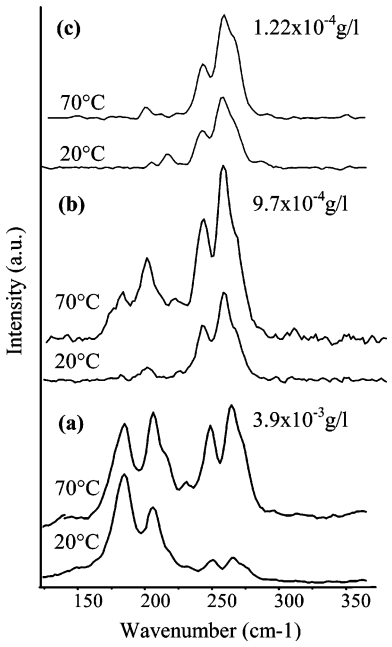

Figure 5. Raman spectra at 20 and 70 °C of the RBMs of the 1:0.001 (0.1 wt % mass fraction) concentration of PmPV at (a) 9.7×10^{-3}, (b) 3.9×10^{-3}, and (c) 1.22×10^{-3} g/L.

developed for a 1:1 interaction, and thus, this value for this mass fraction is used for comparison.

The RBMs were examined at the concentrations shown in Figure 4 (at a 0.1% SWNT mass fraction) down to a concentration of 1.22×10^{-4} g/L. As the concentration is decreased the polymer acts to debundle the nanotubes and therefore at each concentration the nanotubes have varying degrees of aggregation as observed in Figure 4 and implied by the differing RBM profiles of spectra a, b, and c in Figure 5 at 70 °C. This temperature is above the polymer glass transition temperature and it has been demonstrated that in this region the polymer has a significantly reduced interaction with the nanotubes.[16] Such changes in RBM profile due to aggregation are consistent with previous reports for raw tubes.[24] At lower temperatures, as observed for the temperature dependence of the G-line of composites,[16] the increased interaction with the polymer results in a significant change in the RBM profile for concentrations above C_o as shown in Figure 5 (parts a and b) for the case of 20 °C. The change in polymer morphology causes the local environment to change due to both increased interaction with the polymer and tighter packing of the bundles. Thus the change in RBM profile is the result of a change of resonant conditions or alternatively vibrational damping due to tighter bundling and/or interaction with the polymer.

At concentrations below C_o the nanotubes are minimally aggregated or even isolated (Figure 4), and the RBM profile is significantly narrowed from that of the larger bundles and is largely independent of temperature. As the nanotubes are debundled, no changes in either resonant conditions or intertubular damping are observable. Furthermore the interaction with the polymer has little influence on the RBM profile in this temperature range.

It is concluded therefore that whereas at concentrations above C_o the RBM profile at room temperature is significantly influenced by intertubular interactions and polymer binding, and a more representative RBM profile is observed at temperatures above the glass transition temperature of the polymer, at lower concentrations the RBM profile not affected by intertubular interactions is independent of temperature. Thus although a

degree of selectivity may be inferred from low-temperature high-concentration measurements, true selectivity is only observable at concentrations below the critical debundling temperature.

4. Conclusion

Fluorescence spectroscopy is a sensitive probe of polymer−nanotube composite interactions in solutions. Aggregation of polymers is clearly identifiable in pure solutions, and the effect of nanotubes as nanospacers can clearly be seen. The quenching of the polymer PL by tubes and bundles is apparent, and monitoring the concentration dependence can demonstrate the regions in which the polymer/solvent acts to debundle the nanotubes. This suggests that individual nanotubes in a 100% mass fraction are stable below $\sim 1 \times 10^{-4}$ g/L. As the mass fraction is reduced to 1% and 0.01% the saturation point in the plot shifts to higher polymer concentrations of $\sim 5 \times 10^{-4}$ and $\sim 8.5 \times 10^{-4}$ g/L, respectively. The results indicates that choices of composite, i.e., polymer and solvent, have an impact on bundling within these composites. Although aggregation within the polymer/toluene solution is undesirable, it would appear that this system provides stable individual nanotubes at higher concentrations. This result has implications for the determination of diameter distribution and especially size selectivity with Raman spectroscopy. In particular it would suggest that composite spectra should be taken at low polymer concentrations to prevent possible damping of individual tubes within bundles as observed with TD-Raman, or alternatively measurement should be made above the glass transition temperature of the polymer.

Acknowledgment. The FOCAS Institute is funded under the Program for Research in Third Level Institutions (PRTLI), administered by the HEA. S.M.K. acknowledges DIT scholarship support.

References and Notes

(1) Casey, A.; Farrell, G. F.; McNamara, M.; Byrne, H. J.; Chambers, G. *Synth. Met.* **2005**, *153*, 357.

(2) Lupo, F.; Kamalakaran, R.; Scheu, C.; Grobert, N.; Ruhle, M. *Carbon* **2004**, *10*, 1995.

(3) Hedderman, T. G.; Keogh, S. M.; Chambers, G.; Byrne, H. J. *J. Phys. Chem. B* **2004**, *108*, 18860.

(4) Dalton, A. B.; Stephan, C.; Coleman, J. N.; Ajayan, P. M.; Lefrant, S.; Bernier, P.; Blau, W. J.; Byrne, H. J. *J. Phys. Chem. B* **2000**, *104*, 10012.

(5) Keogh, S. M.; Hedderman, T. G.; Farrell, G. F.; Ruether, M.; Gregan, E.; McNamara, M.; Chambers, G.; Byrne, H. J. *J. Synth. Met.* **2005**, *154*, 197.

(6) Steuerman, D. W.; Star, A.; Narizzano, R.; Choi, H.; Ryan, S. R.; Nicolini, C.; Stoddart, J. F.; Heath, J. R. *J. Phys. Chem. B* **2002**, 106.

(7) Lefrant, S.; Baltog, I.; Lamy de la Chapelle, M.; Baibarac, M.; Louarn, G.; Journet, C.; Bernier, P. *Synth. Met.* **1999**, *100*, 13.

(8) Chiang, I. W.; Brinson, B. E.; Smalley, R. E.; Margrave J. L.; Hauge, R. H. *J. Phys. Chem. B* **2001**, *105*, 1157.

(9) Frehill, F.; in het Panhuis, M.; Young, N. A.; Henry, W.; Hjelm, J.; Vos, J. G. *J. Phys. Chem. B* **2005**, *109*, 13205.

(10) in het Panhuis, M.; Maiti, A.; Dalton, A. B.; Van Der Noort, A.; Coleman, J. N.; McCarthy, B.; Blau, W. J. J. *Phys. Chem. B* **2003**, *107*, 478.

(11) Dalton, A. B.; Coleman, J. N.; in het Panhuis, M.; McCarthy, B.; Drury, A.; Blau, W. J.; Paci, B.; Nunzi, J.-N.; Byrne, H. J. *J. Photophys. Photochem. A*: *Chem.* **2001**, *5678*, 1.

(12) Grady, B. P.; Pompeo, F.; Shambaugh R. L.; Resasco, D. E. *J. Phys. Chem. B* **2002**, *106*, 5852.

(13) Valentini, L.; Biagiotti, L.; Kenny, J. M.; Santucci, S. *Comput. Sci. Technol*. **2003**, *63*, 1149.

(14) Probst, O.; Moore, E. M.; Resasco, D. E.; Grady, B. P. *Polymer* **2004**, *45*, 443.

(15) Ryan, K. P.; Lipson, S. M.; Drury, A.; Cadek, M.; Ruether, M.; O'Flaherty, S. M.; Barrow, V.; McCarthy B.; Byrne, H. J.; Blau, W. J.; Coleman, J. N. *Chem. Phys. Lett.* **2004**, *391*, 329.

(16) Keogh, S. M.; Hedderman, T. G.; Gregan, E.; Farrell, G. F.; Chambers, G.; Byrne, H. J. *J. Phys. Chem. B* **2005**, *109*, 5600.

(17) Sugano, M.; Kasuya, A.; Tohji, K.; Saito, Y.; Nishina, Y. *Chem. Phys. Lett.* **1998**, *292*, 575.

(18) Kataura, H.; Kumazawa, Y.; Maniwa, Y.; Umeza, I.; Suzuki, S.; Ohtsuka, Y.; Achiba, Y. *Synth. Met.* **1999**, *103*, 2555.

(19) Rols, S.; Righi, A.; Alvarez L.; Anglaret E.; Almairac R.; Journet C.; Bernier P.; Sauvajol J. L.; Benito A. M.; Maser, W. K.; Munoz. M. M. T.; de la Fuente G. F.; Ginard A.; Ameline J. C. *Eur. Phys. J. B* **2000**, *18*, 201.

(20) Kukovecz, A.; Kramberger, C.; Georgakilas, V.; Prato, M.; Kuzmany, H. *Eur. Phys. J. B* **2002**, *28*, 223.

(21) Souza Filho, A. G.; Jorio, A.; Samsonidze, G.; Dresselhaus, G.; Saito, R.; Dresselhaus, M. S. *Nanotechnology* **2003**, *14*, 1130.

(22) Henrard, L.; Hernandez, E.; Bernier, P.; Rubio, A. *Phys. Rev.* **2001**, *64*, 205402.

(23) Rao, A.; Chen, J.; Richter, E.; Schlecht, U.; Eklund, P. C.; Haddon, R. C.; Venkateswaran, U. D.; Kwon, Y. K.; Tomanek, D. *Phys. Rev. Lett.* **2001**, *86*, 3895.

(24) Heller, D. A.; Barone, P. W.; Swanson, J. P.; Mayrhofer, R. M.; Strano, M. S. *J. Phys. Chem. B* **2004**, *108*, 6905.

(25) Coleman, J. N.; Fleming, A.; Maier, S.; O'Flaherty, S.; Minett, A. I.; Ferreira, M. S.; Hutzler, S.; Blau, W. J. *J Phys. Chem. B* **2004**, *108*, 3446.

(26) Huang, H.; Kajiura, H.; Maruyama, R.; Kadono, K.; Noda, K. *J. Phys. Chem. B* **2006**, *110*, 4686.

(27) Drury, A.; Maier, S.; Rüther, M.; Blau, W. J. *J. Mater. Chem.* **2003**, *13*, 485.

(28) Lynch, P.; O'Neill, L.; Byrne, H. J.; McNamara, M. *SPIE Proc.* **2005**.

(29) Rao, A. M.; Richter, E.; Bandow, S.; Chase, B.; Eklund, P. C.; Williams, K. A.; Fang, S.; Subbaswamy, K. R.; Menon, M.; Thess, R. E.; Dresselhaus, G.; Dresselhaus, M. S. *Science* **1997**, *275*, 187.

(30) Keogh, S. M.; Hedderman, T. G.; Gregan, E.; Farrell, G.; Chambers, G.; Byrne, H. J. *J. Phys Chem. B* **2004**, *108*, 6233.

(31) Huang, F.; Yue, K. T.; Tan, P.; Zhang, S. L.; Shi, Z.; Zhou, X.; Gu, Z. *J. Appl. Phys.* **1998**, *84*, 4022.

(32) Li, H. D.; Yue, K. T.; Lian, L.; Zhou, L. X.; Zhang, S. L.; Shi, Z. J.; Gu, Z. N.; Liu, B. B.; Yang, R. S.; Yang, H. B.; Zou, G. T.; Zhang, Y.; Iijima, S. *Appl. Phys Lett.* **2000**, *76*, 2053.

(33) Ci, L.; Zhou, Z.; Song, L.; Yan, X.; Liu, D.; Yuan, H.; Gao, Y.; Wang, J.; Liu, L.; Zhou, W.; Wang, G.; Xie, S. *Appl. Phys. Lett.* **2003**, *82*, 3098.

(34) Raravikar, N. R.; Keblinski, P.; Rao, A. M.; Dresselhaus, M. S.; Schadler, L. S.; Ajayan, P. M. *Phys. Rev. B* **2002**, *66*, 235424.

(35) Lliev, M. N.; Litvinchuk, A. P.; Arepalli, S.; Nikolaev, P.; Scott, C. D. *Chem. Phys. Lett.* **2000**, *316*, 217.

(36) Karachevtsev, V. A.; Glamazda, A. Y.; Dettlaff-Weglikowska, U.; Kurnosov, V. S.; Obraztsova, E. D.; Peschanskii, A. V.; Eremenko, V. V.; Roth, S. *Carbon* **2003**, *41*, 1567.

(37) Corio, P.; Santos, P. S.; Pimenta, M. A.; Dresselhaus, M. S. *Chem. Phys. Lett.* **2002**, *360*, 557.

(38) Nguyen, T. Q.; Doan, V.; Schwartz, J. *J. Chem. Phys.* **1999**, *110*, 4068.

(39) Keogh, S. M.; Hedderman, T. G.; Gregan, E.; Farrell, G.; Lynch, P.; Chambers, G.; Lyng, F. M.; Byrne, H. J. *SPIE Proc.* **2005**, *5826*, 67.

(40) Hedderman H. G.; Keogh S. M.; Chambers, G.; Byrne, H. J. *J. Phys. Chem. B.* **2006**, *110*, 3895.